Rate of allosteric change in hemoglobin measured by modulated excitation using fluorescence detection

Anthony J. Martino and Frank A. Ferrone
Department of Physics and Atmospheric Science, Drexel University, Philadelphia, Pennsylvania 19104

ABSTRACT We have measured the forward and reverse rates of the allosteric transition of hemoglobin A with three CO molecules bound by using modulated excitation coupled with fluorescence quenching of the DPG analogue, PTS (8-hydroxy-1,3,6 pyrene trisulfonic acid). This dye is observed to bind to the T state with significantly larger affinity than to the R state, and thus provides an unequivocal marker for the molecule's conformational change. The allosteric rates obtained with the fluorescent dye (pH 7.0, bis-Tris buffer) are $(3.4 \pm 1.0) \times 10^3\ s^{-1}$ for the R to T transition and $(2.1 \pm 0.5) \times 10^4\ s^{-1}$ for the T to R transition. This gives an equilibrium constant L_3 of 0.16 ± 0.06. These results provide good agreement with modulated difference spectra calibrated from model compounds, arguing that there is little if any difference in the kinetics observed by the heme spectra and the kinetics of the full subunit motion.

The equilibrium constant between structures (L_3) is smaller in the absence of phosphates than observed in phosphate buffer (0.33). However, the rates of the allosteric transition increase in the absence of phosphates as compared with the corresponding rates in phosphate buffer of $1.0 \times 10^3\ s^{-1}$ and $3.0 \times 10^3\ s^{-1}$. The effects of inorganic phosphates on the equilibrium can be separated from the effects on kinetics. We find that phosphates also affect the dynamic behavior of hemoglobin, and the presence of 0.15 M phosphate can be viewed as raising the transition state energy between R and T conformations by ~0.5 kcal/mol exclusive of the T state stabilization.

Dissociation constants for the dye were measured to be $104 \pm 25\ \mu M$ for unligated T state and $930 \pm 300\ \mu M$ for the fully ligated R state. The best fit equilibrium constant ($125 \pm 40\ \mu M$) for three ligands bound does not differ significantly from that measured without ligands bound. Incidental to the measurement technique is the determination of the rates of binding and release of the dye. The association rate for binding to the T state is large, (at least $4 \times 10^9\ M^{-1}\ s^{-1}$) and may be diffusion limited, while the association and dissociation rates for R state binding, while not determined with precision, are clearly much smaller, of the scale of $10^5\ M^{-1}\ s^{-1}$ for association.

INTRODUCTION

One of the most well known protein structural changes is that executed by the hemoglobin molecule in the course of ligand binding. The ability of hemoglobin to assume either of two quaternary structures, denoted R and T, has been probed by the full range of spectroscopic techniques, and long standing correlations have been established between certain small changes in the optical absorption spectrum and particular quaternary structures. These absorption differences have been almost the sole probe for structural kinetics, beginning with Gibson's classic work in 1959. The correlation of static spectra with structure and function have been assumed to remain valid for kinetics.

Kinetic studies which spectrally follow the events subsequent to photolysis from nanoseconds to seconds (Hofrichter et al., 1985; Murray et al., 1988*a*, *b*) demonstrate the weakness of this assumption. Those experiments resolve three kinetic processes that are identified as geminate rebinding, tertiary relaxation, and quaternary relaxation, with characteristic times from nanoseconds to tens of microseconds, all of which have the same Soret spectral difference shape. Thus the spectral signature alone does not serve to distinguish between local and global protein motion. Techniques such as transient resonant raman spectroscopy, while possessing greater resolution than optical spectra, are again sensitive first and foremost to changes at the heme. (Rosseau and Ondrias, 1983) While more sophisticated techniques such as transient UV resonant Raman coupled to the interfacial residues (Dasgupta et al., 1987) or transient circular dichroism (Ferrone, 1974) can in principle provide unambiguous nonheme structural information, their use has had limited success.

Because quaternary structure is held to be the dominant influence on the heme reactivity (Shulman et al., 1975), this issue might be resolved by observing the rate of ligand binding and so correlating structural change and functional change. Nonetheless, the problem remains of identifying what part of the protein has actually moved.

Anthony Martino's present address is Engineering Physics Laboratory, E. I. Du Pont de Nemours & Co., Wilmington, Delaware 19880-0357.

0006-3495/89/10/781/14 $2.00

For example, Karplus and co-workers (Gelin et al., 1983) have identified an allosteric core to the hemoglobin subunits: is structural relaxation of this core sufficient to change affinity without more global change? A nonheme kinetic probe would clearly be a valuable complement to other detailed kinetic experiments.

In the course of the allosteric structural change in hemoglobin, the beta subunits move significantly far apart to permit the binding of organic polyphosphates, such as the physiological effector, DPG. (Arnone, 1972) The opening of this central cavity is clearly a powerful marker for the structure change, and does not rely on heme absorption. MacQuarrie and Gibson (1971, 1972) found that the fluorescent dye, 8-hydroxy-1,3,6 pyrene trisulfonic acid, PTS, binds preferentially to the T state, in which case its fluorescence is quenched. Displacement by DPG and IHP demonstrated that this probe binds in the central cleft of the hemoglobin tetramer (MacQuarrie and Gibson, 1971, 1972), and this dye has been effectively used as a structural marker in a number of stopped flow and flash photolysis studies (MacQuarrie and Gibson, 1971, 1972, Gibson et al., 1973, Marden et al., 1986).

Here we report the combination of this fluorescent probe with the modulated excitation method to measure the rate of quaternary structure change. Modulated excitation is a perturbation method which uses periodic excitation coupled with phase sensitive detection to extract small structural signals in the presence of larger ligand binding events by appropriate phase tuning of the detection system. (Ferrone and Hopfield, 1976; Ferrone et al., 1985) In the case of fluorescence, this can be realized by taking the photolyzed state as the reference point, so that kinetic evolution from that state can be measured directly. Small excitations are needed to insure that no more than one ligand is removed per tetramer, simplifying the number of assumptions about intermediate states. Because the allosteric structures are energetically close when one ligand has been removed, both forward and reverse allosteric rates are determined in this method. The method has been used with absorption as a probe to follow the structural kinetics of triliganded hemoglobin. This report represents the first use of a nonheme probe to resolve the forward and reverse kinetics of the quaternary structural change.

In outline, this new method is as follows: Fluorescence of the dye is stimulated with a DC source. An AC excitation (photolysis) of the hemoglobin creates an oscillating population in the T state. This population in turn periodically binds and quenches a dye. Thus the dye fluorescence acquires an AC component that can be detected by a lock-in amplifier. The phase and amplitude of this quenched AC fluorescence component contain the information about the kinetics of the steps leading to the binding. Despite the presence of this allosteric effector, the kinetics of allosteric change before effector binding are determined.

THEORY

A perfect fluorescent marker would bind rapidly (and release rapidly) from only one structure. The binding of the probe will of course stabilize the conformation to which it binds, so that the equilibrium between the structures of interest can be disentangled only if the affinity of the probe is known. For such an ideal case, the kinetic description under modulated excitation is essentially that of Ferrone et al. (1985), with fluorescence quenching directly interpreted as the amount of T-state.

At the outset, it is clear that PTS cannot be assumed to be a perfect probe, since it binds to the R state as well as the T state, albeit more strongly to the latter (MacQuarrie and Gibson, 1971, 1972). Moreover, one does not know *a priori* whether the rates of binding and release are faster than the conformational change being measured. In a complete treatment of modulated kinetics with an imperfect probe, a four manifold system is needed, viz. R state, T state, R state with PTS bound (denoted Q) and T state with PTS bound (denoted B). However, the description of the full four manifold system, because of its complexity, does not offer ready insights into the behavior of the probe. Because it will be seen later that simplifications of this kinetic scheme are possible and, in fact, are warranted, the limiting case will be described first for its tutorial value, and then the general theory for the full case will be presented.

The essential description of modulated excitation kinetics followed by absorption has been developed elsewhere (Ferrone et al., 1985). Two quantities were measured in the previous experiment. (a) The tangent of the phase ϕ relative to the excitation gave the response of the molecule to the ligand binding event. (b) The ratio, called Γ, of the out of phase allosteric spectrum to the in phase ligand binding spectrum, gave information about the relative amount of structural change. When Γ is measured as a function of frequency, the kinetics can be determined.

Two new quantities are measured in the fluorescence experiment: the tangent of fluorescent phase θ relative to the ligand rebinding signal, and the magnitude of fluorescence normalized to the total excitation. The limiting case is a two-state description containing states R and B (a T state with PTS bound). The phase relations that contain essential kinetic information are naturally and concisely represented using complex notation. Thus, for example, a

signal shifted in phase by 90° becomes notated as imaginary. Thus we define

$$\tan\theta = \frac{Im\left[\frac{B_3}{R_3 + B_3}\right]}{Re\left[\frac{B_3}{R_3 + B_3}\right]} = -\frac{\omega}{k_{RB} + k_{BR}} \quad (1)$$

and

$$F(\omega) = \left|\frac{B_3}{R_3 + B_3}\right| = \frac{k_{RB}}{\sqrt{(k_{RB} + k_{BR})^2 + \omega^2}} = L_B/(L_B + 1) \text{ at } \omega = 0, \quad (2)$$

where L_B represents the equilibrium constant between R and B, and is equal to k_{RB}/k_{BR}. In this simple description, a plot of $\tan\theta$ vs. ω will be linear with a reciprocal slope of $k_{RB} + k_{BR}$. The low frequency asymptote of F yields L_B thus allowing both forward and reverse rates to be obtained. For comparison, in the absorption measurements, the measured variables are

$$\tan\phi = -\omega/k_R[\mathrm{CO}], \quad (3)$$

where k_R is the rate constant for CO binding to the R structure, and

$$\Gamma = -\frac{\omega k_{RB}}{(k_{RB} + k_{BR})^2 + \omega^2}. \quad (4)$$

This curve peaks when $\omega = k_{RB} + k_{BR}$; at is maximum,

$$\Gamma_{max} = L_B/(2L_B + 2). \quad (5)$$

This, in combination with the low frequency slope or the high frequency asymptote (low or high relative to Γ_{max}) gives full information about the allosteric rates. If the affinity of the probe is known, as measured by its dissociation constant K_d, then the rates of conversion between R and T can be determined. Then it is straightforward to show, assuming dye binding is more rapid than allosteric interconversion, that:

$$k_{RT} = k_{RB}(1 + K_d/[\mathrm{PTS}]) \quad (6)$$

$$k_{TR} = k_{BR}(1 + [\mathrm{PTS}]/K_d) \quad (7)$$

and

$$L_3 = L_B K_d/[\mathrm{PTS}]. \quad (8)$$

The full four manifold model incorporates several assumptions to reduce the potentially large number of free parameters to a manageable set. First it is assumed that the binding of PTS does not significantly alter the R or T state affinity. This means that ligand binding within the B manifold of states is assumed to be the same as ligand binding with T and likewise, ligand binding within the Q manifold is taken to be the same as binding within R. The amount of fully liganded T or B state is assumed to be insignificant so that excitations from these need not be considered. While the essence of this method is to remove only a single ligand per tetramer, the small population of doubly ligated species can contribute noticeable signals when it is out of phase with the triply liganded signals. Hence, we include excitations to the doubly ligated species. It will be seen that a broad range of values is permissible for the parameters used in the analysis of higher excitation, because the effect of multiple excitation is small and thus imprecise. Excitations of more than two ligands per tetramer are assumed not to occur. Excitation rates for the T state are assumed to be double that of the R state (due to the higher quantum yield, or the lower geminate recombination rate). The diagram in Fig. 1 shows this full model, while the full set of equations is presented in the Appendix.

Although the allosteric model is a useful framework for thinking about the details of this problem (Monod et al., 1965, Hopfield et al., 1972), certain precise requirements of the allosteric model are not utilized or required in this formalism. For example, the independence of ligand binding on the number of ligands bound, which is central to the allosteric picture need not hold at all in these descriptions. Indeed, the measurement of L_3 by modulation, for comparison with Lc^3 generated from binding

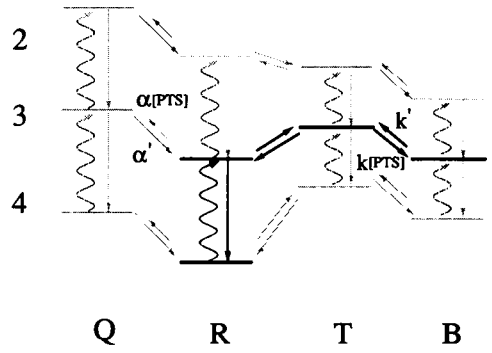

FIGURE 1. Schematic energy level diagram. The vertical direction represents Gibbs free energy. Four structures are shown: R and T, T with PTS bound, denoted B, and R with PTS bound, denoted Q. The numbers on the left describe the number of ligands bound. The simplest model for this experiment is drawn in bold, while the full kinetic description is given in fainter lines. Excitation (denoted A in the text) is shown as a wavy line, ligand rebinding or structure change as a solid line. PTS binding to the T state occurs with a bimolecular rate constant k (unsubscripted) while its binding to the R state has a rate constant α. The release rates are then denoted as k' and α'. The analysis does not presuppose any uphill or downhill relationship between states. Because only ~1% of the hemes are photolyzed, species with fewer than two ligands bound were not considered in the analysis.

curves can provide an independent test of that very hypothesis. Thus, while we shall identify structures based on the equilibrium allosteric end points as R or T, the thermodynamic linkage to those structures is not at all a given in this study.

In terms of the general (four states) model, the four observables in this experiment are defined below. Two measurements, tan ϕ and Γ, are made using the absorption spectra.

Tan ϕ responds to the kinetics of ligand rebinding primarily because the detection system is tuned to an isosbestic between R and T, and thus is insensitive to conformational change. It is defined as:

$$\tan \phi = \frac{Im[B_3 + T_3 + R_3 + Q_3]}{Re[B_3 + T_3 + R_3 + Q_3]}. \quad (9)$$

Γ measures the fraction of excited states out of phase, determined by observing the spectra which are out of phase with the ligand binding process. The spectral shapes and their extinction coefficients are assumed known *a priori*.

$$\Gamma = Im\left[\frac{B_3 + T_3}{B_3 + T_3 + R_3 + Q_3}\right]. \quad (10)$$

Then there are two fluorescence measurements as well, which are made at a single wavelength. Phase and magnitude of the quenched fluorescence are measured. The tan θ phase measurement responds to the fluorescence quenching signal $(B_3 + Q_3 + Q_4)$ measured relative to the phase of the total excitation signal $(B_3 + T_3 + R_3 + Q_3)$.

$$\tan \theta = \frac{Im\left[\frac{B_3 + Q_3 + Q_4}{B_3 + T_3 + R_3 + Q_3}\right]}{Re\left[\frac{B_3 + Q_3 + Q_4}{B_3 + T_3 + R_3 + Q_3}\right]}. \quad (11)$$

The fluorescence magnitude F is defined as the magnitude of the quenched fluorescence signal, relative to the total excitation magnitude.

$$F = \frac{|B_3 + Q_3 + Q_4|}{|B_3 + T_3 + R_3 + Q_3|}. \quad (12)$$

METHODS

Hemoglobin A was prepared as described elsewhere (Ferrone et al., 1985) and placed in pH 7.0, 0.05 M bis tris buffer. Heme concentrations were typically ~1 mM. Sodium dithionite was added to the samples, which had been flushed with CO previously, to give a final concentration of approximately 2 mM. PTS (laser grade, Kodak Laboratory Chemicals, Rochester, NY) was present at concentrations between 150 μM and 1.2 mM, as described below.

The apparatus represents a significant advance over the previously used modulated excitation arrangement. A schematic is shown in Fig. 2. The modulated excitation (photolysis) beam at 573 nm was provided by a Coherent 599 jet stream dye laser, (Coherent, Inc., Palo Alto, CA) pumped by an argon ion laser (model 164 or model 2016; Spectra Physics Inc., Mountain View, CA). The modulated beam then passes through an acoustooptic modulator and impinges upon the sample. A piece of that beam is reflected by a filter, and strikes a FND-100 silicon photodiode, (EG&G Electrooptics, Salem, MA) connected to the modulator driver. The driver is so configured that the diode provides a feedback signal to retain a low distortion sine wave despite modulator nonlinearity, and to stabilize the amplitude of the wave despite variation of the dye laser output. Typical excitation was performed with rhodamine 590 dye in a mixture of ethylene glycol and methanol, lasing at 573 nm. To excite the fluorescent dye, a fraction of the pump laser beam was extracted by reflection from a glass wedge, and dispersed by a prism. The 476 nm line was then selected by beam stops and reflected from the filter in the modulated beam path so that both the DC fluorescence excitation beam and the modulated excitation dye laser beam were collinear in hitting the sample. The photolysis beam was incident on the sample at ~51°, focussed to a spot of gaussian diameter of 350 μm. Typical power at the sample was ~2 mW, where it produced an excitation of 1–1.3% of the hemes. The PTS fluorescence had a broad maximum which peaked at 510 nm, where it was experimentally observed.

For measuring absorbance spectra, a 150 W xenon arc lamp (Osram, George W. Gates, Franklin Park, NY) was dispersed by a monochromator (f/3.8 Monospec 18, Acton Research Instrument and Equipment Services, Acton, MA) set for 2.25 nm resolution, and imaged on the

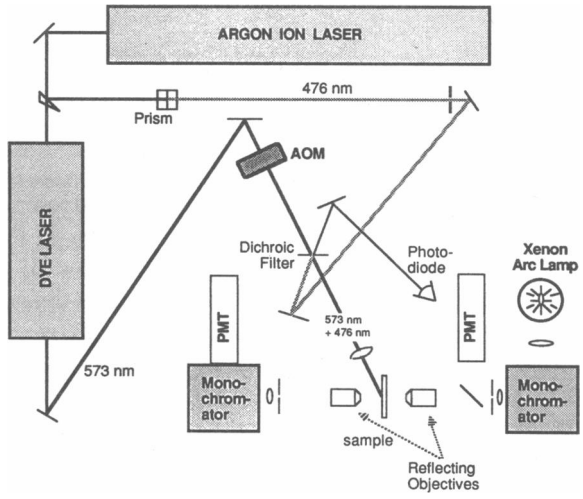

FIGURE 2. Schematic of the apparatus. The argon laser is run multiline to pump the dye laser. About 4% of the pump beam is reflected by a wedge, and dispersed through a prism to select the 476 nm line. This line is then brought to a focus at the sample after reflection from a dichroic mirror. The 573 nm dye laser output, after modulation, passes through the dichroic mirror and is also focussed on the same area, in a much larger spot. A fraction of the modulated dye beam is reflected from the back of the dichroic filter into a photodiode for monitoring and feedback as a controller of the acousto-optic modulator (AOM). For absorbance measurements (AC or DC), the two monochromators are stepped in tandem, while for fluorescence they operate independently. The photomultiplier tube (PMT) near the arc lamp is for reference measurement in absorbance.

sample with a long working distance 15X reflecting microscope objectives (Ealing Corp., Natick, MA). A field diaphragm limited the observation area to a circle of ~23 μM radius on the sample. (This was later replaced with a square aperture of similar size.) The light from the sample was collected with a matching objective, and again masked before being input to a second monochromator identical to the first except for a wider slit width which gave a 9 nm bandpass. The monochromator output was detected by a Hamamatsu R453 photomultiplier (Hamamatsu Inc., Bridgewater, NJ). Both monochromators were computer controlled and could be stepped in tandem or separately. The sample was mounted on a thermoelectric stage (Cambion, Cambridge, MA) with a controller of our own design.

The detection electronics have been previously described. (Ferrone et al., 1985) and were essentially unchanged. For measuring modulated spectra, we adopted a dynamic averaging procedure to insure constant signal to noise ratio: at each wavelength the computer averaged the incoming lock-in amplifier output until the deviations in the average were <5%.

Four modulation measurements (tan ϕ, Γ, tan θ, F) were made at frequencies in the range 200 to 3,000 Hz. These have been described in the theory section, and are experimentally realized as follows: (*a*) tan ϕ. The lockin phase was set to be in phase with the excitation, by stepping the detection monochromator to the laser line, 573 nm, and tuning for zero signal in the out of phase channel. Both monochromators were then set to 436.5 nm, an isosbestic of the R–T difference spectrum (Perutz et al., 1974) Tan ϕ, defined as the negative of the out of phase signal divided by in phase signal was then measured for a series of frequencies. This primarily gives ligand rebinding kinetics. (*b*) Γ. Both monochromators are set to 436.5 nm, and the out of phase signal was nulled by tuning the lockin phase. Once the phase was set, a spectrum was scanned from 400 to 450 nm in 2 nm steps. Both in phase and out of phase spectra are recorded (with the AC output divided by the DC input to normalize for the changes in light transmitted by the sample). The modulation spectra are curve-fit with standard spectra for the ligand rebinding event and the allosteric change. The ratio of the allosteric spectrum in the out of phase channel to the ligand binding spectrum in the in-phase channel is called Γ. The sample absorption spectrum is automatically recorded as a byproduct of each modulation spectrum. (*c*) tan θ. With the lockin tuning described in the preceding section (Γ measurement), the detection monochromator was set to 510 nm, and the input monochromator left at 400 nm. The high voltage on the PMT was increased, and the AC fluorescence signal was monitored. We define tan θ as the ratio of the out of phase to in phase signals for the fluorescence phase tuned to ligand binding. (*d*) F. The magnitude of the modulated fluorescence signal was determined as the square root of the sum of the squares of the in and out of phase signals along with tan θ. The magnitude was normalized both by the dc fluorescence (to account for any drift in the argon laser and to normalize collection geometries) and by the modulated excitation magnitude. The latter is given by the in-phase coefficient of the modulation spectrum, or equivalently by the square root of the sum of the squares of the in and out of phase signals measured as part of tan ϕ.

Dissociation constants for PTS were also determined. For R state hemoglobin a dissociation constant of 930 ± 300 μM was measured by observing the DC fluorescence from a solution of unphotolyzed HbCO as the PTS concentration was changed. For determining the dissociation constant for T state hemoglobin, a steady state photolysis of the HbCO sample was established, and the DC fluorescence quenching measured. For this steady state experiment, the laser was focussed to a smaller spot of gaussian diameter 155 μm. Due to the microscopic sample size, significant steady state photolysis could be effected without appreciable temperature rise. In addition, direct experiments confirmed that temperature had little effect on the dissociation constant measured here. As a final precaution to minimize the effects of temperature, partial photolysis was employed. Photolysis of more than 50% of the hemes was deemed to produce essentially all T state tetramers, based on model calculations using any set of reasonable allosteric parameters. Dissociation constants for PTS from the T state were measured in every experiment as a fundamental control. The average value obtained was 104 ± 25 μM. This value is similar to those obtained by other (MacQuarrie and Gibson, 1972) when differences in ionic strength are taken into account.

Further control experiments demonstrated that there was no significant change in the tan θ in the course of an experiment, and that the fluorescence was linear with excitation intensity in the range employed. Some dye bleaching was noted, amounting to as much as 50% in 7 h. To lessen the impact of this effect, data were not collected in order of modulation frequencies, but the sequence of frequencies was scrambled. This effect accordingly may contribute to some of the variation in the fluorescence magnitude.

RESULTS

Modulated excitation spectra were collected on three samples of HbCO without PTS, but otherwise identical to the PTS-containing samples. Typical results showed an excellent fit to three components: the ligand binding spectrum, the R–T difference spectrum, and an allosterically sensitive spectrum from the CO hemes (Ferrone et al., 1985). As a concise way of describing these results, the spectra were analyzed by singular value decomposition (Golub and Kahan, 1965; Golub and Reinsch, 1970; Shrager and Hendler, 1982) to ascertain the principal components in the data. The in-phase data is shown in Fig. 3 *a*; only one component is significant. The out of phase data had two significant spectra, shown as Fig. 3 *b* and *c*. The spectra at first sight resemble the ligand binding, the deoxy-RT difference spectrum, and a CO-RT difference spectrum which we have previously identified. The fits to the data using the aforementioned spectra as standards are also shown as the dark squares in the figure, and justify the fit of the data to these three standards.

A plot of the relative magnitude of the out of phase signal, denoted as Γ (cf. above) versus frequency, is shown in Fig. 4 *a* averaged for the three experiments without PTS. Ideally such a curve has a single, simple maximum. The zero frequency asymptote should rise linearly in ω while the high frequency asymptote should fall as ω^{-1}. The data shown here have a broad, almost featureless peak. The low frequency rise has been obscured by the effect of multiple excitation to doubly ligated species; the lack of significant falloff can simply mean that high enough frequencies were not used. (The effect of multiple excitations is dealt with thoroughly in the Appendix to Ferrone et al., 1985. A detailed analysis for this experiment shows the same effect.) Nonetheless, the magnitude of the curve (~0.08) can be used as a preliminary gauge for L_3, which must be <~0.2.

Modulated excitation spectra were also collected on six

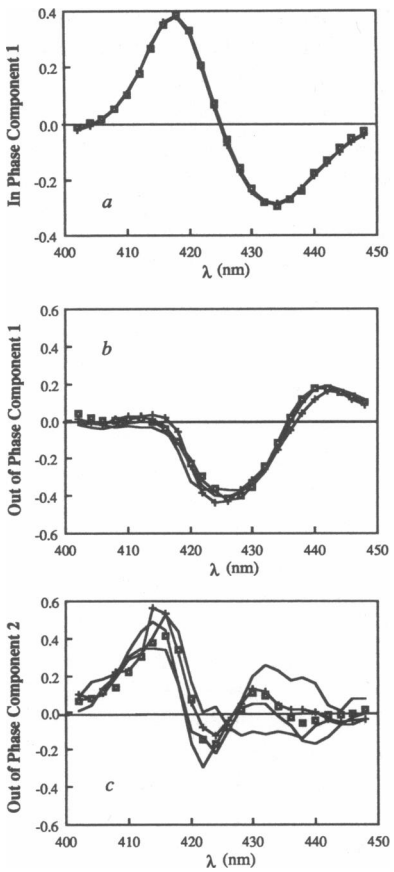

FIGURE 3. Spectra determined by singular value decomposition. Due to computer memory limitations, the spectra were analyzed in groups of ~20. Three groups were taken with PTS, drawn as solid lines, one group was taken without PTS and is drawn as a solid line connecting + symbols. As is evident, there is no significant difference between spectra with and without PTS. To show the quality of the fits of the data to standard spectra, the average of the spectra shown here was fit to the spectra used to fit individual modulation spectra. The fit spectrum is shown as the square symbols, which are not connected by lines. (*a*) In phase spectra. These are dominated by the ligand rebinding event. Only one significant component is seen, of singular value at least 20 times greater than the next spectral component. (*b*) Out of phase spectral component 1. It has singular values of 2.1% of the in-phase spectra (with PTS), and ~1.2% without PTS. It is dominated by the deoxy spectral change that occurs upon the change in quaternary structure. (*c*) Out of phase spectral component 2. The singular value is smaller still, being only 0.6% of the in phase spectrum. This component is dominated by the spectral change at the CO hemes, as discussed in Ferrone et al. (1985). The next smaller component (not shown) was roughly half as small as the component shown in *c*, accounting for at most 0.4% of the in-phase, or 12% of the out of phase spectra.

samples of HbCO with 300 μM PTS. It was apparent that the out of phase signal had increased. We again summarize the spectral data by singular value decomposition. Due to computer memory limitations, we could only analyze 20 spectra at once; hence the data with PTS took three determinations. The curves are also shown in Fig. 3. As is evident there is excellent agreement in spectral shapes with and without PTS. Thus we conclude that no new spectra are introduced in the Soret bands upon addition of PTS. Moreover, the fit of the component spectra remains excellent.

The six experiments with PTS were averaged to show the overall effect on Γ (now denoted as Γ_+) as seen in Fig. 4 *b*. The error bars in Fig. 4 *b* show the effect of the error in fitting the standards to the data as well as the deviation in the averages. A plot of Γ_+ vs. ω (Fig. 4 *b*) showed a

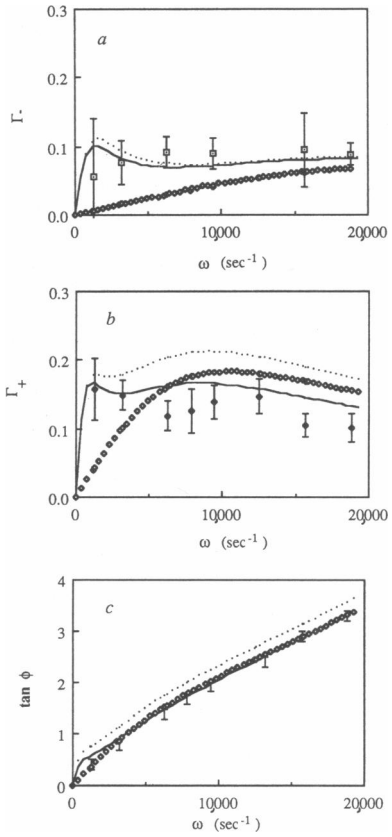

FIGURE 4. Absorbance data, averaged for similar experiments. (*a*) Magnitude of out of phase *R-T* spectrum, divided by the magnitude of the in phase CO-deoxy spectrum as a function of excitation frequency for three experiments without PTS. As described in the text, phase is tuned at 436.5 nm. (*b*) Magnitude of out of phase divided by in phase spectrum as a function of excitation frequency for experiments with 300 μM PTS. (*c*) Tangent of phase of the excitation (measured relative to the laser) as a function fo excitation frequency. In all panels, the dark diamonds represent the prediction of the simplest (rapid equilibration) model based on analysis of the fluorescence data alone. (Parameters employed are listed in Table 1 in column 1.) The dotted line shows the effect of including multiple excitations in the fluorescent-determined description. As can be seen, it increases the low frequency out of phase signal. The solid curve shows the result of the fitting the simplest model to both the absorbance and the fluorescence data. The parameters are in Table 1, column 2. Error bars are the result of both imprecision in the individual data sets and variation between sets.

distinct increase in overall magnitude relative to Γ_- (Fig. 4 *a*) of almost a factor of 2. This is not unexpected since phosphates are known to stabilize the *T* structure. Now there is no evidence of the increasing portion of the graph, but the whole curve decreases slowly with ω.

The tan ϕ measurement changes little upon addition of PTS. The averaged tangent curves with PTS are shown in Fig. 4 *c*. Because this measurement is predominantly sensitive to the ligand binding kinetics, it is a direct indication that the *T*-state stabilization which results in the larger out of phase signal does not lead to significant ligand rebinding from the *T* state, as might occur in the limit of the *T* state becoming a "trap." The presence of significant rebinding produces a pronounced low frequency kink in the tangent according to our calculations. This is also observed experimentally on HbKansas (unpublished results).

Fluorescence data were also gathered for the six experiments with PTS, and the average is shown in Fig. 5. Fig. 5 *a* shows the frequency dependence of the average tan θ measured with 300 μM PTS. The tangent is roughly linear, with the errors at higher frequency arising from the combination of the intrinsic difficulty of the measurement as well as variation between experiments which were averaged. The fact that the tangent does not become large at low frequencies suggests the absence of slow processes in the quenching of fluorescence. Fig. 5 *b* shows the amplitude of the fluoresence, normalized by the sample excitation. The falloff as frequency increases is the expected consequence of the kinetics of allosteric change. Here the large error bars at low frequencies are due to variation between experiments.

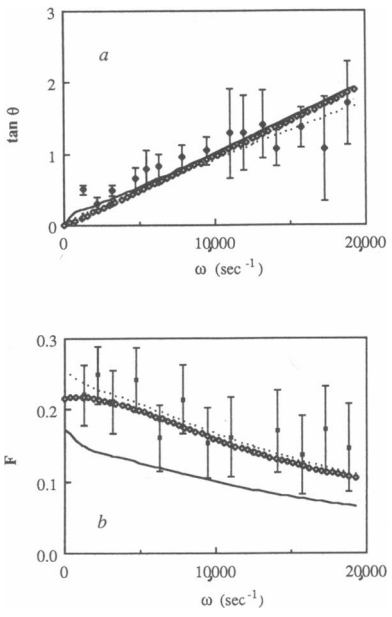

FIGURE 5. Fluorescence data, averaged over all six experiments. (*a*) Tangent of relative phase as a function of frequency. Phase is measured at 510 nm, with tuning to the ligand rebinding signal at 436.5 nm. (*b*) Relative magnitude of the fluorescence quenching as a function of frequency. The magnitude of the fluorescence signal (square root of sum of squares of in phase and out of phase signals) is normalized by the laser intensity and then by the magnitude of the excitation, measured at 436.5 nm. Here the principal contribution to the error bars is the variation between experiments. Symbols for the three theoretical curves in *a* and *b* are as in Fig. 4.

ANALYSIS

In this section we shall first describe the fit of the fluorescence data to the simple, rapid equilibration model, and then compare it with the absorbance data using the same parameters. We will find that the simple model is actually rather accurate, and the parameters also fairly well describe the absorbance data. The closeness of the fit implies that the absorbance and fluorescence are reporting the same events. With this conclusion, we may use both absorbance and fluorescence data to determine a best set of parameters for all the data.

Rapid equilibration analysis

As described in the Theory section (Eq. 1) the slope of the tan θ plot (Fig. 5 *b*) gives the sum of the allosteric rate constants in the simple picture. The best fit slope is 1.1×10^{-4}, giving a sum of rate constants of $8.8 \times 10^3\ s^{-1}$. From Eq. 2 the low frequency limit of *F* gives L_B. If the zero frequency asymptote of the *F* data is taken to be ~0.22, (Fig. 5 *a*) then $L_B = 0.28$. Therefore, $k_{RB} = 1.9 \times 10^3\ s^{-1}$ and $k_{BR} = 6.9 \times 10^3\ s^{-1}$. From Eq. 6 to 9, using the measured values of K_d (104 μM) and [PTS] (300 μM), it is found that $k_{RT} = 2.6 \times 10^3\ s^{-1}$ and $k_{TR} = 2.7 \times 10^4\ s^{-1}$.

The frequency dependence of the fluorescence amplitude, $F(\omega)$, has not yet been used in the analysis. $F(\omega)$ falls off with increasing frequency at a rate that also depends on the allosteric rate constants (Eq. 2). Incorporating this information, a best set of parameters may be generated by nonlinear fitting to the fluorescence data (magnitude and phase) alone. In that case k_{RT} increases to $4.5 \times 10^3\ s^{-1}$ and k_{TR} stays about the same at $2.5 \times 10^4\ s^{-1}$, with L_3 becoming 0.18. This fit is shown in Fig. 5, and the parameters are summarized in Table 1.

These parameters then generate a prediction for the absorbance kinetic data (Γ and tan ϕ). If the absorbance signal is reporting the same structural change, the parameters generated by fluorescence ought to accurately describe the absorbance kinetic data as well. The predicted curve is drawn in Fig. 4 *b*. The maximum for Γ_+ is predicted to be 0.17, which ought to occur at the sum of

the rate constants k_{RB} and k_{BR} ($= 1 \times 10^4\ s^{-1}$). As can be seen in Fig. 4 *b* the fluorescence parameters generate a curve whose magnitude is in agreement with the absorbance data, with its peak lying within the uncertainty of the data points. While it is notable that the low frequency points are not described by this simple model, the presence of multiple excitations will produce just such a low frequency enhancement. The tan ϕ data, describing ligand rebinding is also well fit after adjusting the rate constant for ligand binding to the R structure to be $6.5 \times 10^6\ M^{-1}s^{-1}$.

A second test is to compare the prediction from the fluorescence parameters with Γ_-, the out of phase absorption signal in the absence of PTS (Fig. 4 *a*), given the steady state (zero ligand) value of K_d of 104 μM. The predicted curve is drawn in Fig. 4 *a*. Once again, the predicted maximum of 0.07 agrees with the data, and as seen above, the lower frequency prediction is well below the data. The effect of including multiple excitations[1] is also shown (*dotted line*) in Fig. 4. The strength of the excitation is determined by observing that ~1% of the hemes are excited. The results are not highly sensitive to the parameter choice, as discussed elsewhere (Ferrone et al., 1985), so long as the R_2 to T_2 conversion is rapid, because the rate limiting step is the rebinding within the T manifold. The picture displayed uses $L_2 = 20$, and $k_{RT2} = 2 \times 10^4\ s^{-1}$. As can be seen, the inclusion of multiple excitations makes the Γ plots qualitatively similar to the data, although, particularly with PTS present, the maximum value is now greater.

This simple analysis demonstrates three important conclusions. First, the basic model fits the fluorescence data rather well, affirming the assumptions that the dye is binding rapidly to one structure and that a simple two-state description of the allosteric change is a good starting point. Secondly, the absorbance data is also described by this model using the parameters deduced by fluorescence measurements. This means that to a good approximation, the kinetics seen at the heme and the movement of the full quaternary structure occur in synchrony. Thirdly, the effect of ligation on K_d is small. The K_d determined in steady state photolysis for unliganded molecules is very nearly that required for triply liganded molecules. In view of the first two conclusions, one can ask what the effect would be to attempt to fit both the absorbance and fluorescence data simultaneously, i.e., to assume that both probes report the same event. This is also shown in Fig. 4 and 5, and the parameters are summarized in the second column of Table 1. As can be seen, the fits improve overall.

[1]Despite only photolyzing 1% of the hemes, there is a need for a multiple excitation correction at low frequencies. First of all, only 16% of the excited hemes can cross from R_3 to T_3, so the signal expected is already only a fraction of the excited heme population. Furthermore, at low frequencies these crossovers are mostly in phase and contribute little to Γ, the imaginary out of phase component. On the other hand, multiple excitations provide a signal by the pathway $R_3 \rightarrow R_2 \rightarrow T_2 \rightarrow T_3$ and this signal, being mainly out of phase, can materially increase the size of Γ. In contrast, F and tan θ are not significantly affected. The effect on Γ is discussed in length in the Appendix of Ferrone et al. (1985).

Full analysis

The above conclusions are borne out in a detailed analysis of the four manifold model. In that model there are up to four additional constants: equilibrium constants for PTS binding to the T state (K_d) and to the R state (K_{dR}), as well as kinetic constants for the rate of binding to the T state (labelled simply k) and the rate of binding to the R state (denoted α). We shall first consider two three-manifold variants, i.e., the case where B and T are rapidly equilibrated (but not R and Q), and then the reverse (R and Q in rapid equilibration, but not B and T), and then consider the full four manifold model. Fluorescence and absorbance data are now treated equivalently.

The first case is that of slow binding of PTS to R and fast binding of PTS to the T state. The T and B manifolds remain coalesced, whereas R and Q are not. Thus this allows the allosteric crossing rates to be the rate limiting steps in the transition from R to B, but there is a modification of the fluorescence variable due to the kinetics which allow R to cross to the Q manifold of states. Starting with the parameters used above, a good fit was found with $\alpha = 0.1\ \mu M^{-1}\ s^{-1}$, $K_d = 125\ \mu M$, in which case the χ^2 was 1.14.

It proved impossible to allow the Q and R states to rapidly equilibrate while keeping the kinetics of PTS binding to the T state finite. Any attempt to lower the rate of conversion of T to B led to a worse χ^2, while starting a fit with any finite value of k always improved with larger k until an asymptotic value of ~2,000–4,000 $\mu M^{-1}\ s^{-1}$ (i.e., rapid equilibration) was achieved.

Finally, the complete four manifold model was examined in which binding to the T-state not only competes with allosteric crossing, but the fluorescence measurements must be corrected for the effect of binding PTS to the R-state. Beginning with the best parameters of the prior analysis, with the exception that we lowered k to 10 $\mu M^{-1}\ s^{-1}$, the only way to fit the data was to increase k to 4,000 $\mu M^{-1}\ s^{-1}$, a result which clearly negates the assumption made that the binding of PTS to the T-state is slow. Therefore, the best parameters that were obtained to fit all of the data simultaneously were those already described as rapid equilibration of T and B. These parameters are listed in the last column of Table 1, while the fit is shown in Fig. 6.

It is instructive to consider the intrinsic constraints posed by the data on two critical parameters: k, the rate of dye binding and L_3, the equilibrium between R and T

TABLE 1 Parameters using in fitting data

Parameter	Rapid equilibration: Fluorescence analysis	Rapid equilibration: Global analysis	Finite equilibration, global analysis*	Units
L_3	0.18	0.16	0.16	
k_{RT}	4.5	3.4	3.4	$10^3\ s^{-1}$
k_{TR}	2.5	2.1	2.1	$10^4\ s^{-1}$
K_d	104‡	150	125.	μM
K_{dR}	—	1,500	933.‡	μM
χ^2	2.07§	1.83	0.96	

*Other parameters: (*a*) varied in minimization: $k = 4 \times 10^3\ \mu M^{-1}\ s^{-1}$, $\alpha = 0.1\ \mu M^{-1}\ s^{-1}$, $k_{R34} = 6{,}500\ mM^{-1}\ s^{-1}$ (*b*) roughly adjusted (since the fits are insensitive to their precise values): $k_{RT2} = 2 \times 10^4\ s^{-1}$, $k_{TR2} = 10^3\ s^{-1}$, $k_{RT4} = 26\ s^{-1}$, $A_R = 65\ s^{-1}$ (*c*) obtained from the literature: $k_T = 100\ mM^{-1}\ s^{-1}$ (Parkhurst, 1979).

‡Parameters obtained by independent determination (see text).

§This χ^2 refers to the subset of data used in the fit. The χ^2 for the full data set is 2.84.

structures. Fundamentally k must be large because of the correspondence of the absorbance and fluorescence data, when analyzed independently. A slower kinetic process would affect the phase and magnitude of the fluorescence relative to the absorbance. L_3 has lower and upper bound from the data. The lower limit on the value of L_3 is posed by the magnitude of the fluorescence data F and the Γ absorbance data. Although the magnitude may underestimate the amount of crossover from the R structure, and/or unsuspected kinetic effects may cause less T state to appear, there must be at least enough allosteric conversion to account for the fluorescence and/or absorbance signal seen. Likewise, a kind of counterflow from the Q to R states can decrease the fluorescence magnitude, but not increase it. An upper limit on the value L_3 is set by the shape of the tan ϕ data. For large values of L_3, the B state becomes a trap, with a slow escape rate and hence large values of the tan ϕ at low frequencies. This would cause a pronounced kink in the curve which is not observed.

DISCUSSION

Unlike spectral changes at the heme, or functional alterations such as the binding of ligands with different rates, the measurement of PTS quenching necessarily responds to movement of the subunits. As described above, there is a close correspondence between the events at the heme, and the motion of the subunits. The peak magnitude of

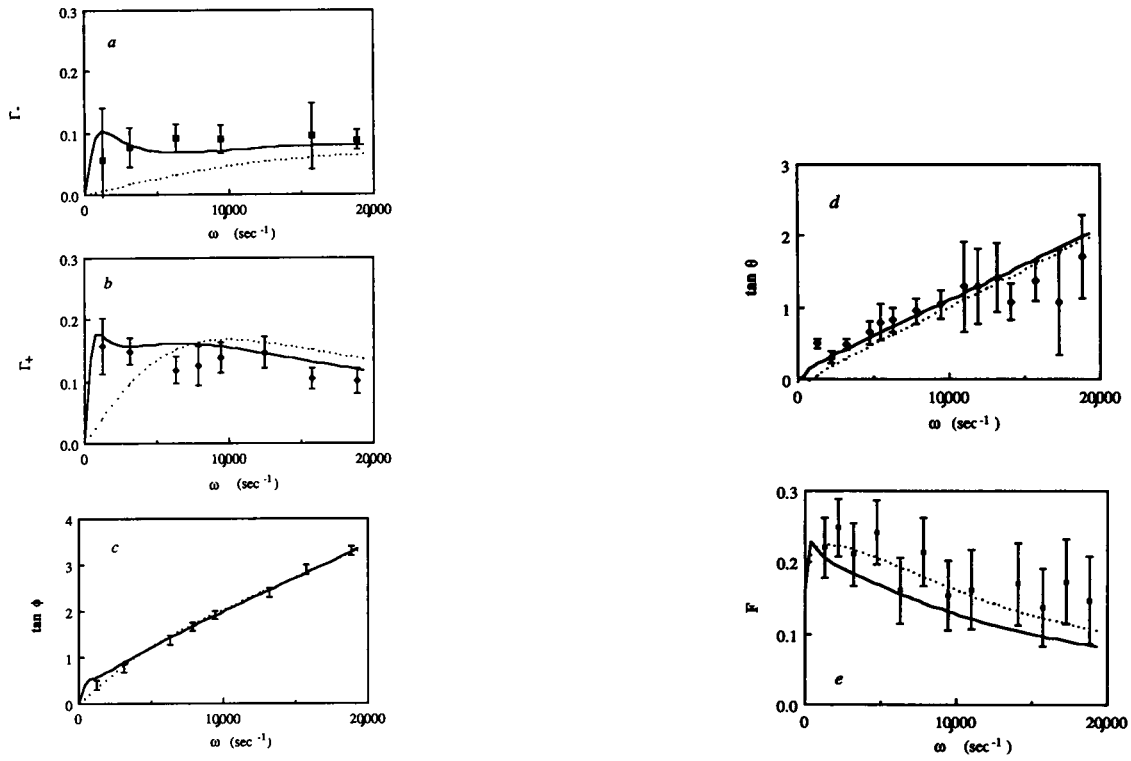

FIGURE 6. Fits of the full model to the absorbance data and fluorescence data of Figs. 4 and 5. Parameters are from Table 1, column 3. The solid curve shows the full description, including multiple excitations; the dotted curve shows the effect of neglecting the multiple excitations (but employing the same parameters.)

the fluorescence signal and the maximum of the out of phase Γ measurement both measure the energy difference between the alternative structures. The close correspondence between these measurements implies that the quaternary structure is fully and tightly coupled to the functional changes seen by the heme. By providing an unequivocal measure of the change in quaternary structure, this experiment demonstrates that the hemoglobin molecule reacts as a fairly rigid object.

Gelin et al. (1983) have advanced the notion that the hemoglobin mechanism involves an allosteric core composed of the heme and proximal histidine, and part of the *F* helix, including the FG corner. In their view, the core comprises a tertiary-level unit. Ligation of a subunit, regardless of the quaternary structure, produces a certain group of changes within the core, which can only be completed upon relaxation of quaternary structure. Our finding of the close coupling (at these timescales) of spectral changes and quaternary motion supports the idea that the core cannot fully relax without the quaternary structure relaxing as well.

It is interesting to compare the present results with previous studies done in phosphate buffer (Ferrone et al., 1985). The known stabilization of the *T* structure in the presence of phosphates accounts for the larger value for L_3 found in that study as compared with the present data taken in bis tris. Stabilizing the *T* structure might have been expected to lower one or both of the quaternary transition rates. It was surprising, then, that both crossing rates were slower in the presence of phosphates. To further explore this, we return to Eqs. 6–8 above. Now K_d may be regarded as the effective phosphate dissociation constant. From Eq. 8, $L_3 = L_B K_d/[PO_4]$. By comparison of the equilibrium constant in the absence of phosphates, $L_3 = 0.16$, with the equilibrium constant obtained in the presence of phosphates, $L_B = 0.33$, we find $K_d/[PO_4] = 0.5$. Since the phosphate concentration is 0.15 M, $K_d = 75$ mM. (This is only an effective K_d because, with more than one binding site, the correct expression is $(K_d/[PO_4])^n = 0.5$, bringing K_d closer to 150 mM). Using Eqs. 6 and 7, the $R \rightarrow T$ rates can then be deduced in the presence of phosphates, effectively before the binding of phosphate ions in the DPG pocket. The resulting $R \rightarrow T$ and $T \rightarrow R$ rates are both twice as slow as those measured in the absence of phosphates. This says that there is a nonallosteric effect of phosphate buffer on the motion of the Hb molecule, at least about its transition state. Fig. 7 shows a transition state picture. The fact that both the rates are increased by the same factor then argues that the free energy of the transition state has been increased (~0.5 kcal).

It is intriguing to ask how this can come about. It is possible that the phosphate ions simply produce a more rigid hydration shell; a second alternative is that there are ions that must be displaced for the structure to switch (e.g., a transient ion binding site). However, it would be remarkable if a number of ions were released in the loss of one structure and the same number were picked up in the other.

The value of K_d for dissociation of PTS determined in steady state (104 ± 25 μM) is very similar to that required in the best fit (125 ± 40 μM). The former value applies to unliganded molecules, while the latter refers to the triligated species. This says that there is little or no effect of ligation on the affinity of the PTS probe, so that PTS binding under these conditions is a good allosteric process (i.e., affinity is approximately constant within a given structure independent of ligation).

The rate of PTS binding is very high, and close to diffusion controlled rates, in agreement with the findings of Marden et al. (1986).[2] This rate proves to be a fundamental difficulty in the natural extension of this experiment, viz., to vary the PTS concentration. Because the PTS binding rate is already virtually instantaneous on the scale of the allosteric transitions, increasing the dye concentration does not help. On the other hand, decreasing the dye concentration, while it would provide kinetic resolution, has the undesirable effect of reducing the signal proportionately, since the dye quenching is what is measured. With the present signal to noise level, this renders the experiment unworkable.

The rapid rate of PTS binding would suggest that DPG binding too ought to be rapid, because the molecular size is similar, the beta crevice opening similar, and the DPG might even be faster due to stronger electrostatic steering. The slowness of the binding to the *R* structure is intriguing. The intuitive picture of the *R*-state binding site being simply a weak site somewhere on the molecular surface

[2]While this work is consistent with the data of Marden et al., (1986) our interpretation of their results is quite different. In their experiment, under partial photolysis, PTS uptake was rapid, and its release was biphasic. They interpreted the slow phase of dye release as the consequence of the switchover from *T* to *R* being rate limited by the slower process of ligand binding to the *T* state, and we agree with that part of the analysis. They further interpreted the fast phase of dye release as rate limited by ligand binding in *R*. We disagree with that interpretation, for without a structure change PTS should not be released and no fluorescent signal observed. Rather, we would interpret the fast phase kinetics as arising from the *T* to *R* process itself. Therefore, contrary to the contention of Marden et al. (1986) the fraction of the fast phase relative to the total fluorescence does not reflect the fraction of intermediate species which have undergone rapid allosteric equilibration, but reflects competition between the *T* to *R* rates (especially T_2 to R_2) and the *T* state ligand binding rate, in which case there is no anomaly vis a vis the two state model. The rates used in our analysis for T_2 to R_2 are 10^3 s^{-1}, which are of the correct scale for the rapid relaxation process observed by Marden et al. (1986). Because many numerical assumptions are required to make this qualitative analysis precise, and since the purpose of our present study is not to test the two state model, we have not pursued this comparison here.

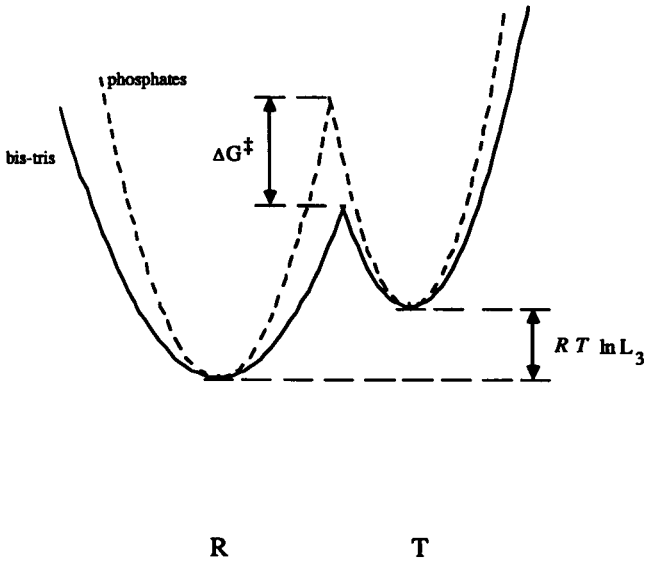

FIGURE 7. Free energy diagram comparing structural change with and without phosphate buffer after structure specific effects are removed. The horizontal coordinate is a schematic reaction coordinate. Using Eqs. 6–8 in the text, an apparent equilibrium constant was deduced for phosphate binding. Thus the dashed curve represents the allosteric conversion (with three ligands bound) before the binding of phosphate ions to the *T* state.

must be replaced by a view in which an infrequent protein fluctuation exposes or creates a binding site for the dye.

APPENDIX

Equations for full manifold calculation

This appendix presents the full system of equations used in the complete model described in the text. The treatment follows the theory of modulated excitation, as developed by Ferrone and Hopfield (1976) and by Ferrone et al. (1985). The population of any state within the framework of an allosteric model (such as that of Hopfield et al. [1972]) will be represented by P_j, where P may be either R or T and where j represents the number of ligands bound. If Q_j represents the population of the jth state of ligation of the corresponding complementary conformer to P (i.e., if P represents R then Q represents T), the kinetic rate equation for the population P_j is given by:

$$\frac{dP_j}{dt} = \left(\frac{dP_{j+1}}{dt}\right)_{\text{photo}} - \left(\frac{dP_j}{dt}\right)_{\text{photo}} - k_{j,j+1}P_j + k_{j-1,j}P_{j-1} + k'_{j+1}P_{j+1} - k'_jP_j + k_{QPj}Q_j - k_{PQj}P_j, \quad \text{(A1)}$$

where $k_{j,j+1}$ is the ligand binding rate from state j to state $j+1$ within the P conformation with the explicit dependence on the ligand concentration suppressed, k'_j is the spontaneous release rate of the ligand from state j, k_{PQj} is the rate of conformational change from the P to the Q conformation at the jth level of ligation, and $(dP_j/dt)_{\text{photo}}$ is the rate of change of state P_j induced by laser photolysis. Since j may run from 0 to 4, for $j+1>4$ and $j-1<0$ the corresponding terms in Eq. A1 do not exist. The rate of photolysis of a sample of hemoglobin, $(dP_j/dt)_{\text{photo}}$, is proportional to the intensity of light absorbed, I_{abs}, *through the relation* $(dP_j/dt)_{\text{photo}} = \phi_q I_{abs}$ where ϕ_q is the quantum efficiency. The absorbed intensity, I_{abs}, for a sample of thickness l, of concentration P_j, and of extinction coefficient ϵ is in turn given by $I_{abs} = I_o - I$, or:

$$I_{abs} = I_o(1 - e^{-2.303\epsilon l P_j}). \quad \text{(A2)}$$

Thus

$$(dP_j/dt)_{\text{photo}} = \phi_q I_o(1 - e^{-2.303\epsilon l P_j}). \quad \text{(A3)}$$

If the population P_j is small, as is assumed to be the case for a weak modulated photolysis, the term in the parentheses may be approximated by a Taylor expansion, keeping terms to first order in P_j. This allows Eqs. 2–4 to be rewritten as:

$$(dP_j/dt)_{\text{photo}} = \phi_q I_o(2.303\epsilon l P_j). \quad \text{(A4)}$$

I_o is the sum of a DC intensity and an AC intensity with modulation frequency ω. The amplitude of the AC variation of the intensity about the DC offset is equal to the DC offset, i.e., $I_o = \langle I \rangle (1 + e^{i\omega t})$ and thus the photolysis rate becomes:

$$(dP_j/dt)_{\text{photo}} = A_P P_j(1 + e^{i\omega t}), \quad \text{(A5)}$$

where $A_P = \phi_q \langle I \rangle 2.303\,\epsilon l$. With the further assumption that since the photolysis is weak, ligation states with two ligands bound or less are not populated, the equations for the rate of change of the individual states are:

$$\frac{dR_3}{dt} = A_R R_4(1 + e^{i\omega t}) - k_{R34}R_3 + k_{TR3}T_3 - k_{RT3}R_3 \quad \text{(A6a)}$$

$$\frac{dT_3}{dt} = A_T T_4(1 + e^{i\omega t}) - k_{T34}T_3 + k_{RT3}R_3 - k_{TR3}T_3 \quad \text{(A6b)}$$

$$\frac{dT_4}{dt} = -A_T T_4(1 + e^{i\omega t}) + k_{T34}T_3 + k_{RT4}R_4 - k_{TR4}T_4 \quad \text{(A6c)}$$

$$\frac{dR_4}{dt} = -A_R R_4(1 + e^{i\omega t}) + k_{R34}R_3 + k_{TR4}T_4 - k_{RT4}R_4. \quad \text{(A6d)}$$

The equations of conservation for the system are:

$$R_3 + T_3 + R_4 + T_4 = C \quad \text{(A6e)}$$

and

$$dC/dt = 0, \quad \text{(A6f)}$$

where C is the total hemoglobin concentration in solution, and the spontaneous off-rates k'_j for CO in both the R and T states are assumed negligible compared to the rates of modulated excitation, A_R and A_T. The population P_j is the sum of a harmonic series:

$$P_j = \sum_{n=0}^{\infty} P_{j,n}\, e^{in\omega t}. \quad \text{(A7)}$$

Upon substituting this relation into the above Eqs. A2–7, one obtains sets of equations in ascending powers of $e^{i\omega t}$, where the powers, n, are the orders of ω. These may then be solved algebraically, first for zeroth order, and then for higher orders. Note that the terms form a hierarchy in which a given order contains only terms of that order or lower order. The first order equations are

$$i\omega R_{3,1} = A_R R_{4,0} + A_R R_{4,1} - k_{R34}R_{3,1} + k_{TR3}T_{3,1} - k_{RT3}R_{3,1} \quad \text{(A8a)}$$

$$i\omega T_{3,1} = A_T T_{4,0} + A_T T_{4,1} - k_{T34} T_{3,1} + k_{RT3} R_{3,1} - k_{TR3} T_{3,1} \quad \text{(A8b)}$$

$$i\omega T_{4,1} = -A_T T_{4,0} - A_T T_{4,1} + k_{T34} T_{3,1} + k_{RT4} R_{4,1} - k_{TR4} T_{4,1} \quad \text{(A8c)}$$

and

$$R_{4,1} = -R_{3,1} - T_{3,1} - T_{4,1}, \quad \text{(A8d)}$$

where the last equation derives from the condition that the sum of all the modulated populations must be zero for consistency. A similar equation results for the 0-order populations when one adds the condition that the total equilibrium populations for all of the states considered must add up to the concentration of hemoglobin in solution, C, i.e.,

$$R_{4,0} = C - R_{3,0} - T_{3,0} - T_{4,0}. \quad \text{(A9)}$$

The small excitation limit implies that $R_{4,0} \gg R_{4,1} \gg R_{3,1}\ R_{2,1} \gg R1,1 \gg R_{0,1}$. Were states R_2, R_1, and R_0 included for a full 10-state model, the small excitation limit would have reduced the resultant first order equations to those of Eq. A8. The situation is the same for the T-manifold. In addition to this approximation, the equilibrium should be heavily in favor of the R-structure at four ligands bound (see for example Shulman et al., 1975). Thus $R_{4,0} \gg T_{4,0}$.

In the full model, PTS binds to both R and T, but with greater affinity for T than for R. This is described by employing the allosteric model for hemoglobin along with additional states for binding of PTS to both the T and R structures. States with two ligands bound were included to act as a correction, which is important for the fit at lower frequencies. Using Eq. A1 yields a set of kinetic differential equations describing the populations of these states. Q represents an R-state molecule with a PTS bound, B represents a T-state molecule with a PTS bound. The equations for the zero-order modulated populations are:

$$0 = A_{2R} R_{30} - (k_{R23} + k_{RT2} + \alpha[\text{PTS}]) R_{20} + k_{TR2} T_{20} + \alpha' Q_{20} \quad \text{(A10a)}$$

$$0 = A_{1R} R_{40} - (A_{2R} + k_{R34} + \alpha[\text{PTS}] + k_{RT3}) R_{30} + k_{R23} R_{20} + \alpha' Q_{30} + k_{TR3} T_{30} \quad \text{(A10b)}$$

$$C = R_{20} + R_{30} + R_{40} + Q_{20} + Q_{30} + Q_{40} + T_{20} + T_{30} + T_{40} + B_{20} + B_{30} + B_{40} \quad \text{(A10c)}$$

$$0 = A_{2Q} Q_{30} - (k_{Q23} + \alpha') Q_{20} + \alpha[\text{PTS}] R_{20} \quad \text{(A10d)}$$

$$0 = A_{1Q} Q_{40} - (A_{2Q} + k_{Q34} + \alpha') Q_{30} + k_{Q23} Q_{20} + \alpha[\text{PTS}] R_{30} \quad \text{(A10e)}$$

$$0 = -(A_{1Q} + \alpha') Q_{40} + k_{Q34} Q_{30} + \alpha[\text{PTS}] R_{40} \quad \text{(A10f)}$$

$$0 = A_{2T} T_{30} - (k_{T23} + k_{TR2} + k[\text{PTS}]) T_{20} + k_{RT2} R_{20} + k' B_{20} \quad \text{(A10g)}$$

$$0 = A_{1T} T_{40} - (A_{2T} + k_{T34} + k_{TR3} + k[\text{PTS}]) T_{30} + k_{T23} T_{20} + k_{RT3} R_{30} + k' B_{30} \quad \text{(A10h)}$$

$$0 = -(A_{1T} + k[\text{PTS}] + k_{TR4}) T_{40} + k_{T34} T_{30} + k_{RT4} R_{40} + k' B_{40} \quad \text{(A10i)}$$

$$0 = A_{2B} B_{30} - (k_{B23} + k') B_{20} + k[\text{PTS}] T_{20} \quad \text{(A10j)}$$

$$0 = A_{1B} B_{40} - (A_{2B} + k_{B34} + k') B_{30} + k_{B23} B_{20} + k[\text{PTS}] T_{30} \quad \text{(A10k)}$$

$$0 = -(A_{1B} + k') B_{40} + k_{B34} B_{30} + k[\text{PTS}] T_{40}. \quad \text{(A10l)}$$

Similarly, the equations for the first order modulated populations are given by:

$$A_{2R} R_{30} = (i\omega + k_{R23} + \alpha[\text{PTS}] + k_{RT2}) R_{21} - A_{2R} R_{31} - \alpha' Q_{21} - k_{TR2} T_{21} \quad \text{(A11a)}$$

$$A_{1R} R_{40} - A_{2R} R_{30} = (i\omega + A_{2R} + k_{R34} + \alpha[\text{PTS}] + k_{RT3}) R_{31} - A_{1R} R_{41} - k_{R23} R_{21} - \alpha' Q_{31} - k_{TR3} T_{31} \quad \text{(A11b)}$$

$$0 = R_{21} + R_{31} + R_{41} + Q_{21} + Q_{31} + Q_{41} + T_{21} + T_{31} + T_{41} + B_{21} + B_{31} + B_{41} \quad \text{(A11c)}$$

$$A_{2Q} Q_{30} = (i\omega + k_{Q23} + \alpha') Q_{21} - A_{2Q} Q_{31} - \alpha[\text{PTS}] R_{21} \quad \text{(A11d)}$$

$$A_{1Q} Q_{40} - A_{2Q} Q_{30} = (i\omega + A_{2Q} + k_{Q34} + \alpha') Q_{31} - A_{1Q} Q_{41} - k_{Q23} Q_{21} - \alpha[\text{PTS}] R_{31} \quad \text{(A11e)}$$

$$-A_{1Q} Q_{40} = (i\omega + A_{1Q} + \alpha') Q_{41} - k_{Q34} Q_{31} - \alpha[\text{PTS}] R_{41} \quad \text{(A11f)}$$

$$A_{2T} T_{30} = (i\omega + k_{T23} + k_{TR2} + k[\text{PTS}]) T_{21} - A_{2T} T_{31} - k_{RT2} R_{21} - k' B_{21} \quad \text{(A11g)}$$

$$A_{1T} T_{40} - A_{2T} T_{30} = (i\omega + A_{2T} + k_{T34} + k_{TR3} + k[\text{PTS}]) T_{31} - A_{1T} T_{41} - k_{T23} T_{21} - k_{RT3} R_{31} - k' B_{31} \quad \text{(A11h)}$$

$$-A_{1T} T_{40} = (i\omega + A_{1T} + k_{TR4} + k[\text{PTS}]) T_{41} - k_{T3} T_{31} - k_{RT4} R_{41} - k' B_{41} \quad \text{(A11i)}$$

$$A_{2B} B_{30} = (i\omega + k_{B23} + k') B_{21} - A_{2B} B_{21} - A_{2B} B_{31} - k[\text{PTS}] T_{21} \quad \text{(A11j)}$$

$$A_{1B} B_{40} - A_{2B} B_{30} = (i\omega + A_{2B} + k_{B34} + k') \cdot B_{31} - A_{1B} B_{41} - k_{B23} B_{21} - k[\text{PTS}] T_{31} \quad \text{(A11k)}$$

$$-A_{1B} B_{40} = (i\omega + A_{1B} + k') B_{41} - k_{B34} B_{31} - k[\text{PTS}] T_{41}, \quad \text{(A11l)}$$

where in the above equations, $k[\text{PTS}]$ and $\alpha[\text{PTS}]$ are the binding rates of PTS to the T-structure and R-structure respectively, and k' and α' are the corresponding release rates from the B and Q structures. The dye is assumed to not affect ligand binding rates. Thus the assumptions for the ligand binding rates are $k_{B34} = k_{T34}$, $k_{Q34} = k_{R34}$, $k_{Q23} = k_{R23} = 2k_{R34}$, and $k_{B23} = k_{T23} = 2k_{T34}$, while for the modulated excitation rates it is assumed that, $A_{2Q} = A_{1Q} = A_{2R} = A_{1R} = A_R$, and $A_{2B} = A_{1B} = A_{2T} = A_{1T} = A_T$. The above equations are easily cast in matrix from:

$$\vec{D} = M\vec{S}, \quad \text{(A12)}$$

where S is the set of populations (either 0 or 1st order) to be determined, M is the matrix which contains all the kinetic rates, and D may be considered the set of driving terms for the set of equations above. The

driving terms for the 0-order populations are mostly 0, whereas for the 1st order populations, they are mostly the 0-order populations adjusted by their respective modulated excitation rates. The exceptions to this observation come from the conservation Eqs. A10 and A11c which set the total population of states equal to the initial tetramer concentration C and the total modulated population (fully ligated as well as partially ligated) to 0, respectively. Inversion of the matrix M to solve for the state populations was accomplished with the IMSL routine for solution of simultaneous equations with complex coefficients.

The curve fitting procedure used to fit the data simultaneously involved minimization of the global reduced χ^2, which was determined by adding the χ^2 values for each of the data plots (without reducing by the number of degrees of freedom) to yield a global sum. This global sum was then divided by the global number of degrees of freedom, which is given by the total number of data points minus the number of parameters varied minus the number of independent equations used for fitting. To assign errors to the parameters used in fitting, once the minimal χ^2 was found, the parameters were varied in both directions until the global χ^2 changed by 1 (Bevington, 1969). A $\chi^2 \leq 1$ means that each of the curves completely hits the error bars in its respective data plot. Thus a change in χ^2 of 1 means that one or more of the curves begins to miss the data. In this way then it was possible to test the sensitivity of each of the parameters varied. The parameters that were varied included k_{RT3}, L_3, L_2, k_{R34}, K_d, and k. The values of k_{RT2} and k_{TR2} were kept large in accord with measurements of others (Sawicki and Gibson [1976, 1977]; Hofrichter et al., [1983, 1985]; Cho and Hopfield [1979]) who found progressively larger rates for the R to T transition as the number of ligands decreases to zero.

We thank Mr. Wolfgang Nadler for generous assistance in the design, construction, and maintenance of the electronics, Dr. Eric Henry for providing us with the routine for singular value decomposition, and Ms. Alison Graf Murray for overall assistance with a myriad of experimental details.

This work was supported by the National Institutes of Health through grant DK30239.

Received for publication 7 March 1989 and in final form 19 June 1989.

REFERENCES

Arnone, A. 1972. X-ray diffraction study of binding of 2,3-diphosphoglycerate to human deoxyhemoglobin. *Nature (Lond.)*. 237:146–149.

Bevington, P. R. 1969. Data Reduction and Error Analysis for the Physical Sciences. McGraw Hill, New York.

Cho, K. C., and J. J. Hopfield. 1979. Spin equilibrium and quaternary structure change in hemoglobin A. *Biochemistry*. 18:5826–5833.

Dasgupta, S., R. A. Copeland, and T. G. Spiro. 1986. Ultraviolet raman spectroscopy indicates fast (<7 ns) R → T-like motion in hemoglobin. *J. Biol. Chem.* 261:10960–10962.

Ferrone, F. A. 1974. PhD Thesis, Princeton University, Princeton, NJ.

Ferrone, F. A., and J. J. Hopfield. 1976. Rate of quaternary structure change in hemoglobin measured by modulated excitation. *Proc. Natl. Acad. Sci. USA*. 73:4497–4501.

Ferrone, F. A., J. Hofrichter, and W. A. Eaton. 1985. Kinetics of sickle hemoglobin polymerization. I. Studies using temperature-jump and laser photolysis techniques. *J. Mol. Biol.* 183:591–610.

Ferrone, F. A., A. J. Martino, and S. Basak. 1985. Conformational kinetics of triligated hemoglobin. *Biophys. J.* 48:269–282.

Gelin, B. R., A. Lee, and M. Karplus. 1983. Hemoglobin tertiary structural change on ligand binding. *J. Mol. Biol.* 171:489–559.

Gibson, Q. H. 1959. The photochemical formation of a quickly reacting form of hemoglobin. *Biochem. J.* 71:293–303.

Gibson, Q. H., A. Riggs, and T. Imamura. 1973. Kinetic and equilibrium properties of hemoglobin Kansas. *J. Biol. Chem.* 248:5976–5986.

Golub, G. H., and J. Kahan. 1965. Calculating the singular values and pseudo-inverse of a matrix. *SIAM (Soc. Ind. Appl. Math.)*. 2:205–224.

Golub, G. H., and C. Reinsch. 1970. Singular value decomposition and least squares solutions. *Numer. Math.* 14:403–420.

Henry, E. R., J. Hofrichter, J. H. Sommer, and W. A. Eaton. 1983. Photolysis of carbonmonoxyhemoglobin and the cooperativity problem. *In* Photochemistry and Photobiology. Vol. 2. A. Zewail, editor. Harwood Academic Publishers, New York. 791–810.

Hofrichter, J., J. H. Sommer, E. R. Henry, and W. A. Eaton. 1983. Nanosecond absorption spectroscopy of hemoglobin: elementary processes in kinetic cooperativity. *Proc. Natl. Acad. Sci. USA*. 80:2235–2239.

Hofrichter, J., E. R. Henry, J. H. Sommer, R. Deutsch, M. Ikeda-Saito, T. Yonetani, and W. A. Eaton. 1985. Nanosecond optical spectra of iron-cobalt hybrid hemoglobins: geminate recombination, conformational changes, and intersubunit communication. *Biochemistry*, 24:2667–2679.

Hopfield, J. H., R. G. Shulman, and S. Ogawa. 1972. An allosteric model of hemoglobin. I. Kinetics. *J. Mol. Biol.* 61:425–443.

MacQuarrie, R., and Q. H. Gibson. 1971. Use of a fluorescent analogue of 2,3-diphosphoglycerate as a probe of human hemoglobin conformation during carbon monoxide binding. *J. Biol. Chem.* 246:5832–5856.

MacQuarrie, R., and Q. H. Gibson. 1972. Ligand binding and release of an analogue of 2,3-diphosphoglycerate from human hemoglobin. *J. Biol. Chem.* 247:5686–5694.

Marden, M. C., E. S. Hazard, and Q. H. Gibson. 1986. Testing the two-state model: anomalous effector binding to human hemoglobin. *Biochemistry*. 25:7591–7596.

Monod, J. C., J. Wyman, and J. P. Changeux. 1965. On the nature of allosteric transitions: a plausible model. *J. Mol. Biol.* 12:88–118.

Murray, L. P., J. Hofrichter, E. R. Henry, M. Ikeda-Saito, K. Kitagashi, T. Yonetani, and W. A. Eaton. 1988*a*. The effect of quaternary structure on the kinetics of conformational changes and nanosecond geminate rebinding of carbon monoxide to hemoglobin. *Proc Natl. Acad. Sci. USA*. 85:2151–2155.

Murray, L. P., J. Hofrichter, E. R. Henry, and W. A. Eaton. 1988*b*. Time-resolved optical spectroscopy and structural dynamics following photodissociation of carbonmonoxyhemoglobin. *Biophys. Chem.* 29:63–76.

Parkhurst, L. J. 1979. Hemoglobin and myoglobin ligand kinetics. *Annu. Rev. Phys. Chem.* 30:503–546.

Perutz, M. F., J. E. Ladner, S. R. Simon, and C. Ho. 1974. Influence of globinstructure on the state of the heme. I. Human deoxyhemoglobin. *Biochemistry*. 13:2163–2173.

Rousseau, D. L., and M. R. Ondrias. 1983. Resonance Raman studies of the quaternary transition in hemoglobin. *Annu. Rev. Biophys. Bioeng.* 12:357–380.

Sawicki, C. A., and Q. H. Gibson. 1976. Quaternary conformational

changes in human hemoglobin studied by laser photolysis of carboxyhemoglobin. *J. Biol. Chem.* 251:1533–1542.

Sawicki, C. A., and Q. H. Gibson. 1977. Quaternary conformational changes in human oxyhemoglobin studied by laser photolysis. *J. Biol. Chem.* 252:5783–5788.

Shrager, R. I., and R. W. Hendler. 1982. Titration of individual components in a mixture with resolution of difference spectra, pKs, and redox transitions. *Anal. Chem.* 54:1147–1152.

Shulman, R. G., J. J. Hopfield, and S. Ogawa. 1975. Allosteric interpretation of haemoglobin properties. *Q. Rev. Biophys.* 8:325–420.